First-Principles Simulation of Amide and Aromatic Side Chain Ultraviolet Spectroscopy of a Cyclic Dipeptide

Zhenyu Li and Shaul Mukamel*

Department of Chemistry, University of California, Irvine, California 92697

Received: July 14, 2007; In Final Form: August 30, 2007

By combining time-dependent density functional theory (TDDFT) and molecular dynamics (MD) simulations, we calculate the ultraviolet absorption and circular dichroism (CD) of a cyclic dipeptide, *cyclo*(L-Pro-D-Tyr), in the 185−300 nm region. The absorption is dominated by the phenol chromophore of tyrosine. The CD spectrum shows both phenol and amide units transitions. A crude coherent two-dimensional ultraviolet spectrum (2DUV) calculated by neglecting the two-excitation states shows a cross-peak between two transitions of the phenol in the tyrosine side chain. Additional cross-peaks between the side chain and the backbone are observed when using a chirality-induced pulse polarization configuration.

I. Introduction

Optical techniques are widely used for the structural characterization and probing ultrafast dynamics of proteins.[1] Infrared spectra monitor the vibrations, whereas visible spectra probe specific chromophores such as porphyrins or retinal. There are two primary types of UV transitions in proteins: the first is the peptide backbone $n\pi^*$ and $\pi\pi^*$ transitions in the far-UV range and the second one is the aromatic side chains. There are only three amino acids with aromatic side chains, phenylalanine (Phe), tyrosine (Tyr), and tryptophan (Trp). According to Platt's notation,[2] there are four valence electronic excitations for each aromatic side chain, namely L_a, L_b, B_a, and B_b. Aromatic side chains are relatively rare, making them easier to characterize, and better local probes for structure. UV resonant Raman excitation profiles are very sensitive to protein structure.[3−7]

Theoretical simulations are necessary for correlating spectra with molecular structure. The exciton model has been widely used for the interpretation of UV spectra of protein.[8,9] The necessary parameters are typically obtained from detailed studies on small model molecules.[10] Thanks to their simplicity and structural rigidity, cyclic dipeptides, also known as diketopiperazines (DKP) or 2,5-piperazinediones, have been an attractive model system for characterizing the interactions between two amide groups.[11−24] The simplest cyclic dipeptide is the unsubstituted DKP, i.e., *cyclo*(Gly−Gly). Its vibrational and electronic spectra have been measured[25−28] and calculated using correlated ab initio techniques.[29] By examining the splitting between the two $\pi\pi^*$ transitions, Hirst et al.[29] concluded that the amide−amide interactions are primary electrostatics.

CD is widely used for probing the secondary structure and folding dynamics of proteins.[30,31] It will be interesting to study chiral substituted DKP, which are optically active (unsubstituted DKP is non-chiral). In this article, we consider the cyclic dipeptide PTDKP composed by proline and tyrosine, i.e., *cyclo*(L-Pro-D-Tyr) [see Figure 1]. Its circular dichroism (CD) spectrum has been measured.[19]

Proline is a unique amino acid, since its side chain is covalently bonded to the nitrogen atom of the peptide backbone. As suggested by CD, the cyclic five-membered ring of proline imposes rigid constraints on the structure of the DKP ring.[19] For unsubstituted DKP, two boat enantiomers lie in a shallow well, separated by a very small barrier corresponding to the planar structure.[29] However, cyclic dipeptides containing proline have a stable boat configuration. On the other hand, the poly peptide of proline can form the PII conformation,[32] which shows a very different CD pattern than α-helix and β-sheet. It is hard to simulate the CD spectra of the PII structure using an exciton model, even with several polarizability parameters.[33] Cyclic dipeptides which contain a proline show a similar CD pattern to the PII structure,[19] making them good candidates for theoretical modeling.

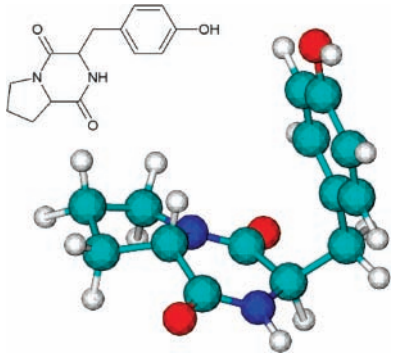

Figure 1. Optimized geometry of PTDKP. Nitrogen (blue), oxygen (red), carbon (green), and hydrogen (white).

The other amino acid in PTDKP, tyrosine, has an aromatic side chain with a phenol chromophore. The phenol L_a excitation is close in energy to the backbone $n\pi^*$ transition, and its B_a and B_b transitions are close to the amide $\pi\pi^*$ transition. The aromatic side chain spectra are very sensitive to their immediate environment, making them excellent probes of protein structure. PTDKP is therefore also an ideal model system for studying backbone−side chain interactions.

Except for the simplest *cyclo*(Gly−Gly), previous theoretical modelings of cyclic dipeptide were carried out using model Hamiltonians. First principles simulations of spectra of molecule of this size are now feasible.[34] In this article, we simulate the spectra of PTDKP by combining time-dependent density functional theory (TDDFT) with first-principles molecular dynamics (MD). Absorption and CD are studied first. Beyond these linear spectroscopic techniques, two-dimensional (2D)

10.1021/jp075515s CCC: $37.00
Published on Web 10/17/2007

coherent third-order optical techniques may reveal additional details.[35−38] Such techniques are becoming available due to the recent development of ultrafast UV laser sources. The cross-peaks in 2DUV spectra may provide a good probe for the backbone−side chain interaction, which may not be probed by CD directly. Previously, we have used a model Hamiltonian to simulate 2DUV of protein. We demonstrated that the technique can distinguish between two different parametrized Hamiltonians both providing a good fit for CD.[39] Here, simulated 2DUV of PTDKP show clear cross-peaks between side chain and backbone. We describe the computational details in section II. The electronic structure, the MD fluctuations, and the simulated UV spectra are presented in section III. Finally, we conclude in section IV.

II. Computational Details

The simulations were performed in three steps. First, a MD simulation is used to generate a trajectory of PTDKP on the ground state potential energy surface. Repeated TDDFT calculations then provide the excited states information at different geometries. Finally, the spectra are simulated using the sum over states expressions for the response functions.[35]

Molecular Dynamics Simulations. We solve the classical equations of motion of the nuclei in 1 fs time steps by means of the Verlet leapfrog algorithm,[40] as available in the FROG module[41] of the TURBOMOLE program suite.[42] SV(P) basis set[43] was used. Energies and forces were evaluated with the BP86 functional[44,45] in combination with the RI-J approximation[46,47] and a small quadrature grid (size 2).[48] Implicit solvent effects were taken into account by the COSMO model[49] using the dielectric constant of water. The Nose-Hoover thermostat[50] is included to run constant temperature MD. First, a 2 ps trajectory is generated at 800 K, and 20 snapshots are taken from this trajectory. Starting from these initial configurations, 20 trajectories were launched at 300 K. Each trajectory comprised 2000 1 fs time steps, corresponding to a total simulation time of 40 ps. After an initial 200 step equilibration, we sampled structural parameters and computed the UV spectra every twenty steps, for a total of $N = 1800$ snapshots.

Time-Dependent Density Functional Calculations. Using TDDFT calculations for the 1800 snapshots, we extracted 30 excitations to cover the 185−300 nm range. The hybrid density functional of Perdew, Burke, and Ernzerhof (PBE0)[51] was used. It contains 25% of Hartree−Fock exchange, is more robust for higher excitation energies,[52] and is less susceptible to charge-transfer error than other functionals. SV(P) basis set was used. Our test on one snapshot indicated that SV(P) gave similar result with larger TVZP basis set in the frequency range considered. The TDDFT response calculations were based on ground state DFT wavefunctions with COSMO continuum solvent model. All calculations were carried out with TURBOMOLE.

Spectra Simulation. Spectra were calculated from the response functions,[35] by using the SPECTRON package.[53] Inhomogeneous broadening due to slow fluctuations is assumed. Fluctuations are taken from fully quantum-mechanical Born−Oppenheimer MD simulations, where ensemble averages are replaced by time averages.[54,55] For each snapshot, the response function is calculated by sum over the lowest 30 excited states. Transition energies, transition dipoles, and magnetic dipoles of these excited states to the ground state are obtained from the TDDFT. There is a minor difference between the velocity and length representations of a transition dipole, the mean value was used in our calculations. Two-exciton states are not available from linear response TDDFT within the adiabatic approximation,[56,57] and were neglected. This does not affect absorption and CD spectra but should affect the 2DUV signals.

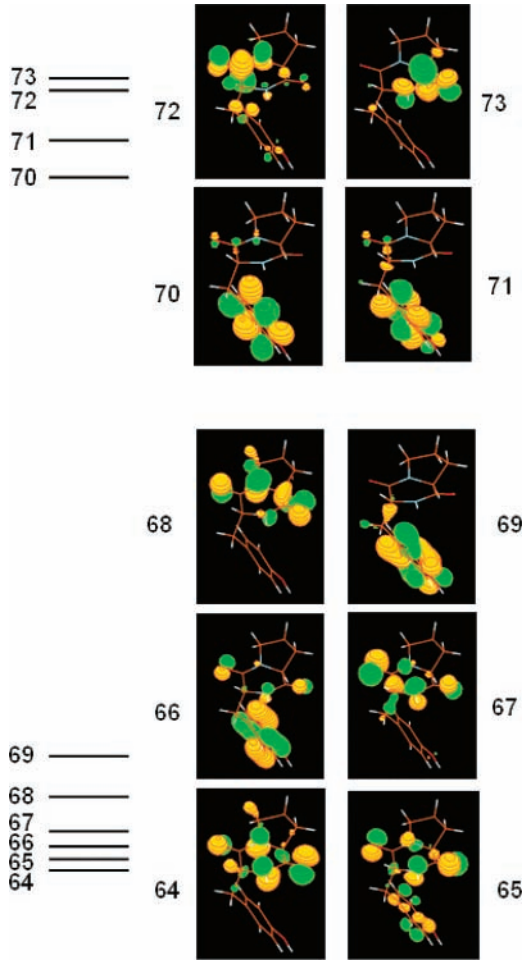

Figure 2. Molecular orbitals and their energy levels. The highest occupied molecular orbital (HOMO, orbital 69) is at −6.48 eV, and the lowest unoccupied molecular orbital (LUMO, orbital 70) is at −0.41 eV.

III. Results and Discussion

A. Geometry and Electronic Structure. The optimized PTDKP geometry with solvent effects included by the COSMO continuum model is shown in Figure 1. As suggested by previous force field calculations,[19] the DKP ring in the optimized structure has a boat configuration. Its mean deviation from a plane is 0.096 Å. The phenol ring is almost planar, with a mean deviation 0.002 Å. For such systems, it has been suggested that, due to interactions between aromatic and peptide π systems, the folded conformer predominates for several solvents and temperatures.[20] Instead of using the two torsion angles γ_1 and γ_2[58] to describe the folding configuration, we used a single parameter, the folding angle θ between the two least-squares planes of the DKP ring and the phenol ring. The optimized geometry gives $\theta = 59.0°$.

Based on the optimized geometry, the electronic structure of PTDKP is calculated with the PBE0 hybrid density functional. A 6.07 eV gap between the highest occupied molecular orbital (HOMO) and the lowest unoccupied molecular orbital (LUMO) is obtained. As shown in Figure 2, the HOMO (orbital 69) is a π orbital within the phenol ring of tyrosine. LUMO (orbital 70) and LUMO+1 are both antibonding π orbitals of the phenol ring. L_b and L_a represent transitions from HOMO to these two orbitals. We shall label the Pro-Tyr peptide unit and the Tyr-

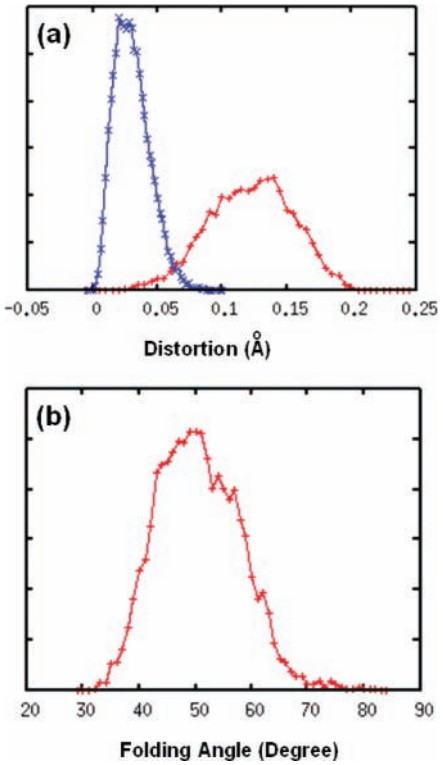

Figure 3. (a) Distributions of the distortions of the dipeptide ring Δ_1 (red) and the phenol ring Δ_2 (blue). (b) Distribution of the folding angle θ.

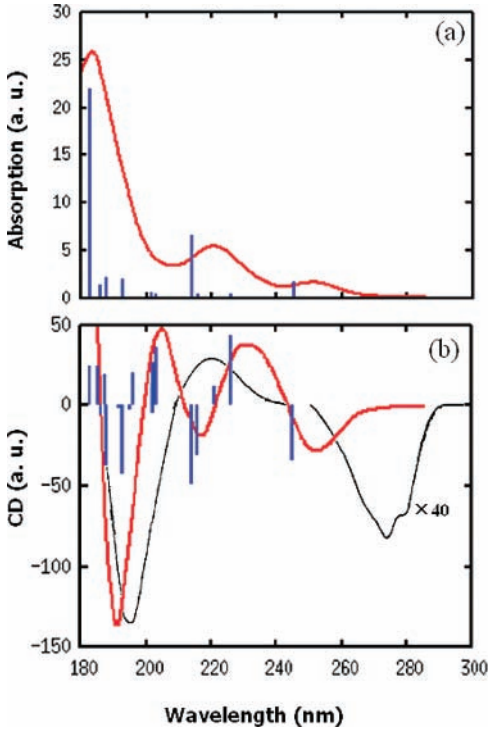

Figure 4. Simulated (a) absorption and (b) circular dichroism of PTDKP. Black line is the experimental CD.[19] The intensity of the experimental CD in the 250−300 nm range is multiplied by 40. Stick spectra are calculated from optimized PTDKP geometry.

Pro peptide unit as 1 and 2, respectively. Orbital 68 is then a combination π_2 and n_1. Orbital 67 is a combination of n_2 and π_1. Orbital 66 is mainly the phenol π orbital, with small contributions from n_1 and n_2 electrons. Orbital 65 is more complicated, it is a combination of n_2, n_1, π_1, and π_{phenol}. For unoccupied orbitals, the mixing between the two peptide units is smaller than in the lower occupied states. Orbital 72 is π_2^*, and orbital 73 is π_1^*.

B. Structural fluctuations from ab Initio Molecular Dynamics. Geometry optimization may depend on the starting configuration. To generate a good ensemble of structures, we carried out an MD simulation. CD measurements suggest that the PTDKP conformation does not vary strongly for different solvents.[19] The Continuum solvent model should thus be adequate.

Since the DKP and phenol rings are the chromophores, we shall mainly consider fluctuations of the rigidity of these two rings and their folding configuration. The ring rigidity is measured by the mean deviation of the six atoms on the ring from their least-squares plane. These will be denoted Δ_1 (DKP) and Δ_2 (phenol). The distributions of the mean deviations of these two rings are displayed in Figure 3. As expected, the phenol ring is almost planar, with mean Δ_2 about 0.03 Å. It is also very rigid, and the variance of Δ_2 is only 0.014 Å. The dipeptide ring is more flexible, with a mean value and variance of Δ_1 0.12 and 0.032 Å, respectively. The folding angle θs centered at 50.6° (variance 7.48°) indicates a folded configuration. No jump from folded to unfolded configurations is observed in our MD simulations.

C. Absorption and CD Spectra. The simulated absorption spectrum is depicted in Figure 4A. A 150 cm^{-1} Lorentzian broadening (fwhm) is added to each snapshot. There are mainly three peaks in the spectrum. We can assign these peaks from the stick spectrum by examining the excitation configurations in the optimized geometry. The absorption is dominated by the phenol side chain of tyrosine. The strongest ~184 nm peak at the blue side is the B_a transition. The second ~221 nm peak is the L_a state, and the weakest ~252 nm peak corresponds to the L_b transition. The peptide $n\pi^*$ transitions are forbidden. One of the two peptide $\pi\pi^*$ transitions is covered by the phenol B_a peak, and the other has higher energy, outside the frequency range of our plot.

The CD spectrum simulated with the same protocol is displayed in Figure 4B. Its main features agree with experiment.[19] At the blue side, ~192 nm, there is a strong negative peak, which mainly comes from the $\pi_2\pi_2^*$ transition within the Tyr-Pro peptide unit. This is the main feature of all proline-containing cyclic dipeptides. It is interesting to note that the oscillator strength of B_a is much larger than $\pi_2\pi_2^*$, but the rotatory strength is weaker. Therefore, by combining the absorption and CD spectra, we can determine the transition energies of both states. The red side is dominated by the negative L_b peak, which is stronger and blue-shifted compared to experiment. The measured intensity of L_b strongly depends on the type of solvent,[19] and the difference in intensity between our calculation and experiment may be caused by the continuum model used for the solvent. Another possible reason is the underestimated frequency of the TDDFT charge transfer state, as will be discussed later.

Between $\pi_2\pi_2^*$ and L_b, there are three additional states, namely the two peptide $n\pi^*$ states and the phenol L_a state. The two $n\pi^*$ states are almost degenerate. In the experiment,[19] only one positive peak is observed between the two negative peaks, and there is a small frequency range around 250 nm where no experimental data are available. Madison et al.[19] had assigned this positive peak to both $n\pi^*$ and L_a. Our simulated CD show two positive and one negative peak between $\pi_2\pi_2^*$ and L_b. The stick spectrum analysis indicates that the positive 234 nm CD peak is mainly $n\pi^*$, the other positive peak is mainly a charge transfer state between the dipeptide and the phenol rings, and

TABLE 1: TDDFT Ensemble Averaged Transition Frequencies and Experimental CD Peak Positions[a]

	L_b	L_a	B_a	$n\pi^*$	$\pi\pi^*$
expt	280	225	–	215	195
TDDFT	252	221	184	231	192

[a] Both are in nm.

the negative peak is L_a. Our TDDFT calculations give an incorrect order for L_a and $n\pi^*$ and shift a high-energy charge transfer state to the experimental frequency range. TDDFT is well-known to underestimate charge transfer state energies, compared with higher level of theory.[59,60] In our TDDFT calculations, the charge transfer states mix with the $n\pi^*$ and L_a states. This may be the reason why their order is reversed.

The negative L_a CD peak is slightly shifted with respect to the corresponding absorption peak. This is because the negative L_a CD peak is close to the positive $n\pi^*$ peak, and they interfere. Therefore, the $n\pi^*$ CD peak should be slightly blue-shifted compared to the transition energy (a reasonable estimate is 231 nm). By combining the absorption and the CD, we obtained ensemble averaged TDDFT transition energies for all transitions in the experimental frequency range, and it is shown in Table 1. These will be used in the next section to assign cross-peaks in 2D signals.

D. Two-Dimensional Electronic Correlation Spectroscopy. A 2D photon echo (2DPE) experiment uses three pulses with wavevectors $\mathbf{k}_1$, $\mathbf{k}_2$, and $\mathbf{k}_3$, which interact with the molecule to generate a coherent signal in the direction $\mathbf{k}_s = -\mathbf{k}_1 + \mathbf{k}_2 + \mathbf{k}_3$.[35−38] There are three time delays (t_1, t_2, and t_3) between the three incoming pulses and the signal pulse. 2D correlation plots of the signals are plotted as Fourier transforms with respect to t_1 and t_3, and we set $t_2 = 0$. Different polarization and wavevector configurations are denoted by $\mu_4\mu_3\mu_2\mu_1(\alpha_4\alpha_3\alpha_2\alpha_1)$, where μ_i is the polarization direction of field i and α_i is its wavevector direction. The α_i indices will be omitted when the signal does not depend on wavevectors of the field.

We have simulated the two-dimensional photon echo spectrum of PTDKP by calculating third-order response function (eq 3.6 of ref 61). The imaginary part of the signal for the all parallel *xxxx* pulse polarization configuration is shown in the top panel in Figure 5. Along the diagonal line, as expected, the 2D signal is very similar to linear absorption (see Figure 6a) and is dominated by two peaks from phenol L_a and B_a transitions. Most interesting is the cross-peak observed between these two transitions. The diagonal 2DPE peaks are broad along the diagonal direction, but narrower in the antidiagonal direction. This characteristic selective elimination of inhomogeneous broadening along the antidiagonal direction in 2DPE allows us to extract information about spectral fluctuations and dephasing.

Chirality induced 2DUV signals are extension of CD, which have been predicted to be a powerful technique.[62,63] These signals also depend on the wavevectors of the fields. We adopted the configurations where all fields propagate along *z*, and simulated the real part of the chiral 2DPE *xxxy*(*zzzz*) signal. The chiral signal is weaker than the nonchiral one, but it contains more information. As shown in Figure 6b, the diagonal section of the chiral 2DPE is similar to CD spectrum. It is interesting to note that the charge-transfer peak in the simulated CD at 205 nm does not appear in the diagonal spectrum of the *xxxy*(*zzzz*) signal. In the nondiagonal region, we see many cross-peaks. The upper triangle region shows cross-peaks between $n\pi^*$ and L_a, $n\pi^*$ and $\pi\pi^*$, and $n\pi^*$ and B_a. In the lower triangle region, we have cross-peaks between $n\pi^*$ and $\pi\pi^*$, L_a and $\pi\pi^*$, and $\pi\pi^*$ and B_a.

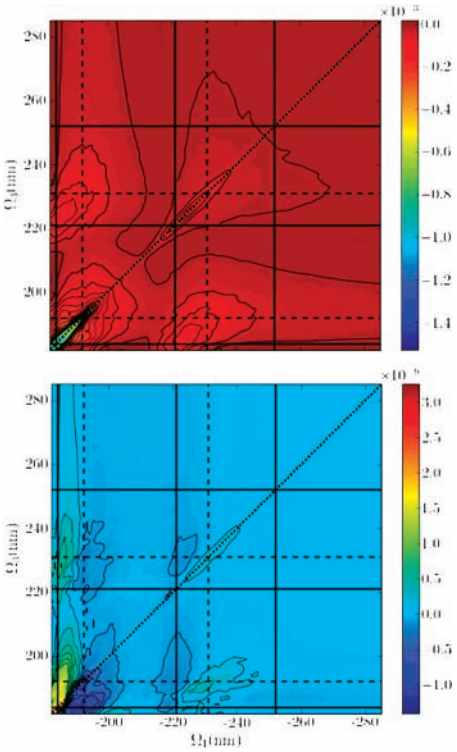

Figure 5. Top: Simulated *xxxx* 2DUV signal. Diagonal line is marked by dotted line. The three solid grid lines indicate energies of phenol side chain transitions B_a (184 nm), L_a (221 nm), and L_b (252 nm), respectively. The two dashed grid lines correspond to energies of backbone transitions $\pi_2\pi_2^*$ (192 nm) and $n\pi^*$ (231 nm). Bottom: chiral The *xxxy*(*zzzz*) spectrum.

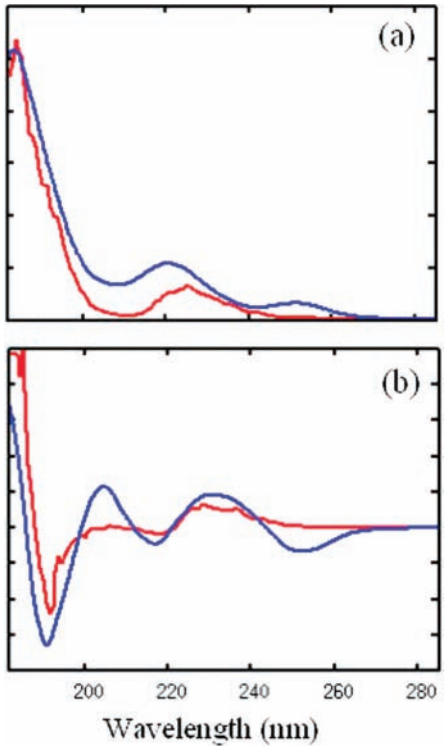

Figure 6. (a) Absorption (red) and the minus diagonal section (blue) of the *xxxx* 2DUV signal. (b) CD spectrum (red) and the diagonal section (blue) of the chiral *xxxy*(*zzzz*) signal.

An extremely interesting feature of the chirality induced 2DUV signals is that they show cross-peaks between the aromatic side chain and the backbone, which are absent in the nonchiral *xxxx* signal. Cross-peaks reflect the interactions

between transitions. Therefore, this UV technique can directly probe the interaction between side chains and backbone. Amino acids with aromatic chromophores are relatively rare in proteins and can thus provide a site specific information, as is done by isotopic labeling in the infrared spectroscopy.

In our simulations of 2DUV, the two-excitation states are not included, since they are not available from TDDFT. This may be justified if two-exciton couplings are very large, shifting these states outside the spectral range of interest. At this point, we cannot tell how good this approximation is for PTDKP. It is a formidable challenge, however, to calculate the two-excitation states accurately with an affordable computational cost. Higher level electronic structure techniques which can describe the two-excitation states, such as full configuration interaction (CI), multireference CI (MRCI), second-order multiconfigurational perturbation theory (CASPT2), and couple-cluster singles and doubles (CCSD), are only feasible for very small systems. Some attempts to go beyond the adiabatic approximation in TDDFT to include double excitations have been made recently.[56,64] 2DUV could provide a powerful probe for two excitation states.[65]

IV. Conclusions

The electronic structure and spectra of PTDKP are studied at the ab initio TDDFT level. This cyclic dipeptide mainly assumes the folded configuration in water. The absorption is dominated by the phenol side chain excitations. The simulated CD reproduces the two negative experimental peaks, whereas an extra charge transfer state appears between them. TDDFT gives the wrong order for $n\pi^*$ and L_a transitions. The simulated photon echo spectrum shows peaks from phenol L_a and B_a states, and their cross-peak. Chiral 2DPE further enhances the resolution and reveals numerous additional features. Several cross-peaks are observed. We expect the possibility to observe 2DUV cross-peaks between backbone and side chains to be very useful for probing protein structure and folding dynamics.

Acknowledgment. We thank Dr. Darius Abramavicius and Dr. Filipp Furche for many helpful discussions. This work was supported by the National Institutes of Health Grant GM59230 and the National Science Foundation Grant CHE-0446555.

References and Notes

(1) Hammes, G. G. *Spectroscopy for the Biological Sciences*; Wiley: New York, 2005.
(2) Platt, J. R. *J. Chem. Phys.* **1949**, *17*, 484.
(3) Lednev, I. K.; Karnoup, A. S.; Sparrow, M. C.; Asher, S. A. *J. Am. Chem. Soc.* **1999**, *121*, 8074.
(4) Lednev, I. K.; Karnoup, A. S.; Sparrow, M. C.; Asher, S. A. *J. Am. Chem. Soc.* **1001**, *123*, 2388.
(5) Asher, S. A.; Mikhonin, A.; Bykov, S. *J. Am. Chem. Soc.* **2004**, *126*, 8433.
(6) Ahmed, Z.; Beta, I. A.; Mikhonin, A. V.; Asher, S. A. *J. Am. Chem. Soc.* **2004**, *127*, 10943.
(7) Mikhonin, A. V.; Asher, S. A. *J. Am. Chem. Soc.* **2006**, *128*, 13879.
(8) Bayley, P. M.; Nielsen, E. B.; Schellman, J. A. *J. Phys. Chem.* **1969**, *73*, 228.
(9) Woody, R. W. *J. Chem. Phys.* **1968**, *49*, 4797.
(10) Besley, N. A.; Hirst, J. D. *J. Am. Chem. Soc.* **1999**, *121*, 9636.
(11) Balasubramanian, D.; Wetlaufer, W. B. *J. Am. Chem. Soc.* **1966**, *88*, 3449.
(12) Urry, D. W. *Annu. Rev. Phys. Chem.* **1968**, *19*, 477.
(13) Kopple, K. D.; Ohnishi, M. *J. Am. Chem. Soc.* **1969**, *91*, 962.
(14) Sletten, E. *J. Am. Chem. Soc.* **1970**, *92*, 172.
(15) Strickland, E. H.; Wilchek, M.; Horwitz, J.; Billups, C. *J. Biol. Chem.* **1970**, *245*, 4168.
(16) Karle, I. L. *J. Am. Chem. Soc.* **1972**, *94*, 81.
(17) Karle, I. L.; Ottenheym, H. C. *J. Am. Chem. Soc.* **1974**, *96*, 539.
(18) Snow, J. W.; Hooker, T. M., Jr. *J. Am. Chem. Soc.* **1975**, *97*, 3506.
(19) Madison, V.; Young, P. E.; Blout, E. R. *J. Am. Chem. Soc.* **1976**, *98*, 5358.
(20) Young, P. E.; Madison, V.; Blout, E. R. *J. Am. Chem. Soc.* **1976**, *98*, 5365.
(21) Sammes, P. G.; Weedon, A. C. *J. Chem. Soc., Perkin Trans.* **1979**, *1*, 3048.
(22) Bowman, R. L.; Kellerman, M.; Hohnson, W. C., Jr. *Biopolymers* **1983**, *22*, 1045.
(23) Fleischhauer, J.; Grotzinger, J.; Kramer, B.; Kruger, P.; Wollmer, A.; Woody, R. W.; Zobel, E. *Biophys. Chem.* **1994**, *49*, 141.
(24) Besley, N. A.; Brienne, M.-J.; Hirst, J. D. *J. Phys. Chem. B* **2000**, *104*, 12371.
(25) Kaya, K.; Nagakura, S. *Theor. Chim. Acta* **1967**, *7*, 124.
(26) Nielsen, E. B.; Schellman, J. A. *J. Phys. Chem.* **1967**, *71*, 2297.
(27) Kaya, K.; Nagakuru, S. *J. Mol. Spectrosc.* **1972**, *44*, 279.
(28) Song, S.; Asher, S.; Krimm, S.; Shaw, K. D. *J. Am. Chem. Soc.* **1991**, *113*, 1155.
(29) Hirst, J. D.; Persson, B. J. *J. Phys. Chem. A* **1998**, *102*, 7519.
(30) Nakanishi, K.; Berova, N.; Woody, R. W. *Circular Dichroism Principles and Applications*; VCH: New York, 1994.
(31) Fasman, G. D. *Circular Dichroism and the Conformational Analysis of Biomolecules*; Plenum: New York, 1996.
(32) Creighton, T. E. *Proteins, structures and Molecular Properties*, 2nd ed.; W. H. Freeman: New York, 1993.
(33) Woody, R. W. Private communication.
(34) Frelek, J.; Kowalska, P.; Masnyk. M.; Kazimierski, A.; Korda, A.; Woznica, M.; Chmielewski, M.; Furche, F. *Chem. Eur. J.* **2007**, *13*, 6732.
(35) Mukamel, S. *Principles of Nonlinear Optical Spectroscopy*; Oxford University Press: New York, 1995.
(36) Mukamel, S. *Ann. Rev. Phys. Chem.* **2000**, *51*, 691.
(37) Asplund, M. C.; Zanni, M. T.; Hochstrasser, R. M. *Proc. Natl. Acad. Sci. U.S.A.* **2000**, *97*, 8219.
(38) Brixner, T.; Stenger, J.; Vaswani, H. M.; Cho, M.; Blankenship, R. E.; Fleming, G. R. *Nature* **2005**, *434*, 625.
(39) Li, Z.; Abramavicius, D.; Zhuang, W.; Mukamel, S. *Chem. Phys.* **2007**, in press. DOI: 10.1016/j. chemphys.2007.03.029.
(40) Verlet, L. *Phys. Rev.* **1967**, *159*, 98.
(41) Elliott, S. D.; Ahlrichs, R.; Hampe, O.; Kappes, M. M. *Phys. Chem. Chem. Phys.* **2000**, *2*, 3415.
(42) Ahlrichs, R.; Bar, M.; Haser, M.; Horn, H.; Kolmel, C. *Chem. Phys. Lett.* **1989**, *162*, 165.
(43) Schafer, A.; Horn, H.; Ahlrichs, R. *J. Chem. Phys.* **1992**, *97*, 2571.
(44) Becke, A. D. *Phys. Rev. A* **1988**, *38*, 3098.
(45) Perdew, J. P. *Phys. Rev. B* **1986**, *33*, 8822.
(46) Eichkorn, K.; Treutler, O.; Ohm, H.; Haser, M.; Ahlrichs, R. *Chem. Phys. Lett.* **1995**, *242*, 652.
(47) Eichkorn, K.; Weigend, F.; Treutler, O.; Ahlrichs, R. *Theor. Chem. Acc.* **1997**, *97*, 119.
(48) Treutler, O.; Ahlrichs, R. *J. Chem. Phys.* **1995**, *102*, 346.
(49) Klamt, A.; Schurmann, G. *J. Chem. Soc. Perkin Trans.* **1993**, *5*, 799.
(50) Hoover, W. G. *Phys. Rev. A* **1985**, *31*, 1695.
(51) Perdew, J. P.; Ernzerhof, M.; Burke, K. *J. Chem. Phys.* **1996**, *105*, 9982.
(52) Adamo, C.; Scuseria, G. E.; Barone, V. *J. Chem. Phys.* **1999**, *111*, 2889.
(53) Zhuang, W.; Abramavicius, D.; Hayashi, T.; Mukamel, S. *J. Phys. Chem. B* **2006**, *110*, 3362.
(54) Allen, M. P.; Tildesley, D. J. *Computer Simulation of Liquids*; Oxford University Press: Oxford, 1987.
(55) Frenkel, D.; Smit, B. *Understanding Molecular Simulation: From Algorithms to applications*, 2nd ed.; Academic Press: San Diego, CA, 2001.
(56) Maitra, N. T.; Zhang, F.; Cave, R. J.; Burke, K. *J. Chem. Phys.* **2004**, *120*, 5932.
(57) Casida, M. *J. Chem. Phys.* **2005**, *122*, 54111.
(58) IUPAC *Biochemistry* **1970**, *9*, 3471.
(59) Dreuw, A.; Head-Gordon, M. *Chem. Rev.* **2005**, *105*, 4009.
(60) Oakley, M. T.; Hirst, J. D. *J. Am. Chem. Soc.* **2006**, *128*, 12414.
(61) Abramavicius, D.; Mukamel, S. *Chem. Rev.* **2004**, *104*, 2073.
(62) Abramavicius, D.; Mukamel, S. *J. Chem. Phys.* **2006**, *124*, 34113.
(63) Abramavicius, D.; Zhuang, W.; Mukamel, S. *J. Phys. B: At. Mol. Opt. Phys.* **2006**, *39*, 5051.
(64) Cave, R. J.; Zhang, R.; Maitra, N. T.; Burke, K. *Chem. Phys. Lett.* **2004**, *389*, 39.
(65) Yang, L.; Mukamel, S. *Phys. Rev. Lett.* **2007**, submitted.